mathematics

MDPI

Article

Dynamics of Activation and Regulation of the Immune Response to Attack by Viral Pathogens Using Mathematical Modeling

Ledyz Cuesta-Herrera [1,*,†], Luis Pastenes [2,†], Ariel D. Arencibia [3,†], Fernando Córdova-Lepe [1,†] and Cristhian Montoya [4,†]

[1] Departamento de Matemática, Física y Estadística, Facultad de Ciencias Básicas, Universidad Católica del Maule, Talca 3480112, Chile; fcordova@ucm.cl
[2] Departamento de Biología y Química, Facultad de Ciencias Básicas, Universidad Católica del Maule, Talca 3480112, Chile; lpastenes@ucm.cl
[3] Centro de Biotecnología en Recursos Naturales, Facultad de Ciencias Agrarias y Forestales, Universidad Católica del Maule, Talca 3480112, Chile; aarencibia@ucm.cl
[4] Escuela de Ciencias Aplicadas e Ingeniería, Universidad EAFIT, Medellín 050022, Colombia; cdmontoyaz@eafit.edu.co
* Correspondence: lcuesta@ucm.cl
† These authors contributed equally to this work.

Abstract: In this paper, a mathematical model is developed to simulate the activation of regulatory T lymphocytes dynamics. The model considers the adaptive immune response and consists of epithelial cells, infected cells, free virus particles, helper and cytotoxic T lymphocytes, B lymphocytes, and regulatory T lymphocytes. A mathematical analysis was carried out to discuss the conditions of existence and stability of equilibrium solutions in terms of the basic reproductive number. In addition, the definitions and properties necessary to preserve the positivity and stability of the model are shown. The precision of these mathematical models can be affected by numerous sources of uncertainty, partly due to the balance between the complexity of the model and its predictive capacity to depict the biological process accurately. Nevertheless, these models can provide remarkably perspectives on the dynamics of infection and assist in identification specific immunological traits that improve our comprehension of immune mechanisms. The theoretical results are validated by numerical simulations using data reported in the literature. The construction, analysis, and simulation of the developed models demonstrate that the increased induced regulatory T lymphocytes effectively suppress the inflammatory response in contrast to similar cells at lower contents, playing a key role in maintaining self-tolerance and immune homeostasis.

Keywords: coronavirus; immune system; regulatory T lymphocytes; SARS CoV-2; mathematical model

MSC: 37N25; 92-10

Citation: Cuesta-Herrera, L.; Pastenes, L.; Arencibia, A.D.; Córdova-Lepe, F.; Montoya, C. Dynamics of Activation and Regulation of the Immune Response to Attack by Viral Pathogens Using Mathematical Modeling. *Mathematics* **2024**, *12*, 2681. https://doi.org/10.3390/math12172681

Academic Editors: José Leonel Linhares da Rocha and Daniele Fournier-Prunaret

Received: 31 July 2024
Revised: 20 August 2024
Accepted: 23 August 2024
Published: 28 August 2024

1. Introduction

In December 2019, an outbreak of coronavirus pneumonia (COVID-19) was reported in Wuhan, China [1–5], showing on 13 April 2023 more than 761 million confirmed cases and more than 7 million deaths worldwide, due to severe acute respiratory syndrome coronavirus 2 (SARS-CoV-2), which is an enveloped, unsegmented, positive-sense RNA virus belonging to the genus betacoronavirus [6,7].

SARS-CoV-2 has undergone more than ten thousand unique mutations recorded compared to the reference genome [8,9]. The rapid spread and global transmission of COVID-19 provides the virus with substantial opportunities for the continued mutation of SARS-CoV-2 that generates multiple variants, but most of them have the same features [10–15].

Taking into account the global emergence evidenced [16], it is necessary to build in-host mathematical models involving the most recent advances in the knowledge of the

immune response to the virus, showing in detail the interaction among SARS-CoV-2 with the immune response.

It should be noted that even in the case of the non-productive interaction of the virus with the cell, SARS-CoV-2 signaling can regulate the cellular activity, and this leads us to talk about the infection of T lymphocytes with SARS-CoV-2 [17–19] since this is accompanied by significant changes in the functioning of the immune system and its potential ability to infect T lymphocytes [18,20].

The regulatory T lymphocytes (Tregs) subpopulation plays a key role in the maintenance of self-tolerance and immune homeostasis. Natural Tregs (nTregs) mature in the thymus, and their primary task is to suppress the immune response to self-antigens, whereas inducible Tregs (iTregs) are formed in the later stages of any immune response, and they are designed to limit excessive inflammation, thus preventing tissue damage by products.

Several studies point to Tregs lymphocytes as a possible target for SARS-CoV-2 [20,21]. Therefore, this paper presents a new mathematical model of Tregs lymphocytes activation, which shows that the expansion of induced Tregs lymphocytes effectively suppresses the inflammatory response, playing a key role in maintaining self-tolerance and immune homeostasis. Furthermore, a new contribution is demonstrated, focusing on mathematical models representing infection within the human host, in which the existence and stability conditions for equilibrium solutions in terms of the basic reproductive number are established. The theoretical results are validated by numerical simulations using data reported in the literature.

The rest of the study is organized as follows: Section 2 presents the mathematical model, while Section 3 focuses on the mathematical analysis of the model and the discussion of the numerical results. Section 4 presents the conclusions drawn from the main results obtained and, finally, Appendices A–C describes the mathematical context related to the study problem.

2. Methods

Model

In this section, we present the mathematical modeling related to the activation of the immune system, variables and parameters in the dynamics of viral infection, and cellular immune response to SARS-CoV-2 virus. The main consideration is the activation of regulatory T lymphocytes leading to the homeostasis of the organism. The initial dynamics of the problem is represented by System (1), for which quotients are incorporated to control the maximal stimulus of infected cells (I) on Helper T lymphocytes (H), thus evidencing a decrease in infected cells.

On the other hand, where referring to an instant t, $E = E(t)$ is the number of epithelial cells (susceptible) [cells], $I = I(t)$ is the number of infected cells [cells] activated by the virus to initiate viral replication, and $V = V(t)$ is the number of free viral particles $[copies/ml]$. There is a presentation of previously phagocytosed antigens by cells of the reticuloendothelial system to specific H lymphocytes, which multiply and achieve clonal expansion. These Helper T lymphocytes release cytokines that direct a cellular and humoral response for the elimination of SARS-CoV-2 [22].

At least 20 different antigens have been identified among the virus proteins; however, approximately one-fifth are capable of generating an effective cellular and neutralizing the antibody response [23,24].

In addition, the activation of cytotoxic T lymphocytes (C) results in their clonal expansion and subsequent targeting of infected cells to induce programmed cell death or apoptosis. This process halts the release of new virions and eliminates existing virions within the infected cell (I), thus preventing their release into the extracellular environment. Furthermore, the activation of B lymphocytes leads to the production and secretion of antibodies that block viral entry into cells and enhance the virus's elimination through phagocytosis. While both immune responses are crucial for controlling the infection, the

cellular response is considered more decisive due to the strictly intracellular nature of the viral replication [25]. Thus, the described biological behavior is modeled in System (1) using a set of ordinary differential equations (ODEs):

$$\begin{cases} E' = g_E - \left(d_E + \tau_E \frac{V}{V+\zeta_{VE}}\right) E, \\ I' = \tau_E \frac{VE}{V+\zeta_{VE}} - \left(d_I + \tau_I \frac{C}{C+\zeta_{CI}}\right) I, \\ V' = \nu I - \left(d_V + \tau_V \frac{B}{B+\zeta_{BV}}\right) V, \\ H' = g_H - \left(d_H - \tau_H \frac{I}{I+\zeta_{IH}}\right) H, \\ C' = g_C - \left(d_C - \tau_C \frac{H}{H+\zeta_{HC}}\right) C, \\ B' = g_B - \left(d_B - \tau_B \frac{H}{H+\zeta_{HB}}\right) B. \end{cases} \tag{1}$$

The definitions of the initial model variables and parameters, along with their biological interpretations, are given in Table 1.

Since maintaining self-tolerance and immune homeostasis requires effective suppression of the inflammatory response against similar cells with lower content, the activation of regulatory T lymphocytes (R), an important subpopulation of T cells that exert immunosuppressive effects is considered.

Recent studies have shown that the number of R lymphocytes is significantly reduced in patients with COVID-19, affecting several aspects, such as weakening the effect of inflammatory inhibition, causing an imbalance in the Treg/Th17 ratio, and increasing the risk of respiratory failure [8,17,26,27].

A better understanding of the role of R lymphocytes will allow advances in symptom management and the possibility of delaying or preventing disease progression in patients with COVID-19. These cells are made up of several subpopulations of T lymphocytes delimited by their expression of markers (CD4+, CD8+, etc.), ensuring immune homeostasis by substantially suppressing CD4+ cells, as well as playing a role in reducing the immune response after the infection has ended [17,27]. Therefore, the behavior of regulatory T lymphocytes is modeled within a robust mathematical framework that is both predictive and explanatory. The importance of including this variable in System (1) is described as follows:

Helper and cytotoxic T lymphocytes and B lymphocytes curves do not achieve a sufficiently rapid decline in the simulations. In the immune response to infection, there is a more rapid decline in the number of active lymphocytes after antigen clearance is achieved.
There is an over-dependence on cell turnover parameters d_H, d_C and d_B. It is not possible to adjust cell turnover parameters to achieve a further decline in lymphocyte populations after infection. We have the restriction that τ_H, τ_C and τ_B do not exceed deaths to avoid explosive growth.

Therefore, it is considered necessary to include an additional variable reflecting the role of regulatory T lymphocytes in the regulation of the immune system as shown in System (2):

$$\begin{cases} E' = g_E - \left(d_E + \tau_E \frac{V}{V+\zeta_{VE}}\right) E, \\ I' = \tau_E \frac{VE}{V+\zeta_{VE}} - \left(d_I + \tau_I \frac{C}{C+\zeta_{CI}}\right) I, \\ V' = \nu I - \left(d_V + \tau_V \frac{B}{B+\zeta_{BV}}\right) V, \\ H' = g_H - \left(d_H - \alpha \frac{I}{I+d} + \rho_H R\right) H, \\ C' = g_C - \left(d_C - \tau \frac{H}{H+l} + \rho_C R\right) C, \\ B' = g_B - \left(d_B - \beta \frac{H}{H+l} + \rho_B R\right) B, \\ R' = g_R - (d_R - \tau_R H) R, \end{cases} \tag{2}$$

where parameters ρ_H, ρ_C, and ρ_B are numbers of R lymphocytes that inhibit the effect of other lymphocytes per unit of time.

Table 1. Description of the variables and parameters of System (1).

Variables	**Description**
E	Epithelial cells
I	Infected cells
V	Free viral particles
H	Helper T lymphocytes
C	Cytotoxic T lymphocytes
B	B lymphocytes
Parameters	**Description**
d_E	Epithelial cell death rates
d_I	Infected cell death rates
d_V	Degradation rate of free viral particles
d_H	Helper T lymphocytes death rate
d_C	Cytotoxic T lymphocytes death rate
d_B	B lymphocytes death rate
g_E	Epithelial cell generation rate
g_H	Helper T lymphocytes production rate
g_C	Cytotoxic T lymphocytes production rate
g_B	B lymphocytes production rate
ν	Replication rate of viral particles free of infected cells
τ_E	Probability of epithelial cell infection per viral particle
τ_I	Lysis effect on infected cells
τ_V	Neutralization effect on free viral particles
τ_H	Activation effect on helper T lymphocytes
τ_C	Activation effect on cytotoxic T lymphocytes
τ_B	Activation effect on B lymphocytes
ζ_{VE}	Amount of virus at which half of the maximum infection rate is reached.
ζ_{CI}	Number of cytotoxic T lymphocytes at which half of the maximum clearance rate is reached
ζ_{BV}	Number of B lymphocytes at which half of the maximum neutralization rate is achieved.
ζ_{IH}	Number of infected cells at which half of the maximum activation rate is reached
ζ_{HC}	Number of helper T lymphocytes at which half of the maximum proliferation rate is reached
ζ_{HB}	Number of helper T lymphocytes at which half of the maximum proliferation rate is reached

Note that in System (3), quotients are included in the state variables H, C, B and R to control the number of lymphocytes at which the maximum rate of each of their various effector functions is reached. This behavior is illustrated in a schematic diagram shown in Figure 1:

$$\begin{cases} E' = g_E - \left(d_E + \tau_E \frac{V}{V+\zeta_{VE}}\right) E, \\ I' = \tau_E \frac{VE}{V+\zeta_{VE}} - \left(d_I + \tau_I \frac{C}{C+\zeta_{CI}}\right) I, \\ V' = \nu I - \left(d_V + \tau_V \frac{B}{B+\zeta_{BV}}\right) V, \\ H' = g_H - \left(d_H - \tau_H \frac{I}{I+\zeta_{IH}} + \rho_H \frac{R}{R+\zeta_{RH}}\right) H, \\ C' = g_C - \left(d_C - \tau_C \frac{H}{H+\zeta_{HC}} + \rho_C \frac{R}{R+\zeta_{RC}}\right) C, \\ B' = g_B - \left(d_B - \tau_B \frac{H}{H+\zeta_{HB}} + \rho_B \frac{R}{R+\zeta_{RB}}\right) B, \\ R' = g_R - \left(d_R - \tau_R \frac{H}{H+\zeta_{HR}} + \rho_R\right) R. \end{cases} \tag{3}$$

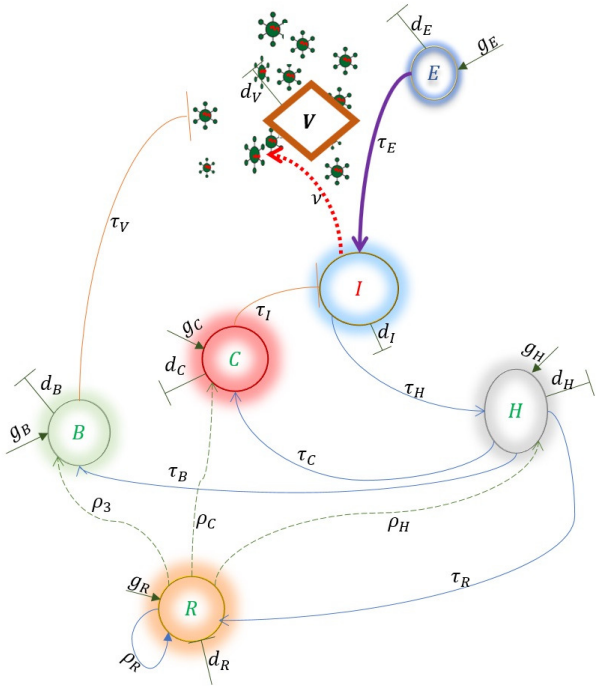

Figure 1. Schematic of the mechanism of the immune response incorporating the interaction between E, V, I and leading to the activation of H, C, B, and R lymphocytes. Associated with System (3).

3. Results and Discussion

We present a mathematical immunology model during the activation of the immune system, involving epithelial cells and their interaction with free SARS-CoV-2 virus particles. Tracking the functioning of different lymphocytes allows us to identify their behavior over time after symptom onset. In particular, the model suggests that activation of regulatory T lymphocytes enhances the inhibition of effector functions of the immune system, ensuring homeostasis. Our analysis is consistent with experimental data indicating that approximately 5 to 15 days after symptom onset is the peak of the immune response when there is an interaction between the SARS-CoV-2 virus and the immune System [28–37].

Figures 2–5 reflect what happens to an individual who is in homeostasis. That is, the initial condition starts for the variables E, H, C, B and R in the infection-free equilibrium.

Note that, in the trajectories, the number of epithelial cells starts from its homeostatic value g_E/d_E, then decreases according to the intensity of the infection, and then recovers its value.

At the first moment of the first viral load in System (3), i.e., $V(0) > 0$, without infected cells $I(0) = 0$, then, the disease has a chance to take off (settle) as

$$I'(0) = \tau_E \frac{V(0)}{V(0) + \zeta_{VE}} \frac{g_E}{d_E} > 0.$$

This also indicates that if the initial viral load is very large, then $I'(0) = \tau_E g_E/d_E$, the maximum number of epithelial cells that can be infected per unit time.

Figure 2 illustrates the biological behavior observed once free virus particles (V) enter the organism through the nasal cavity and interact with epithelial cells (E), facilitating their entry via cellular receptors, leading to infected cells (I). Thus, we can envision a set of epithelial cells undergoing cellular turnover depending on their generation rate (g_E) and death rate (d_E), the latter being a result of apoptosis that begins after completing their life cycle.

In addition, Figure 2 shows that around the third day, epithelial cells (E) decrease, leading to an increase in infected cells as symptoms begin. This, in turn, triggers the activation of H lymphocytes, which subsequently activate B and C lymphocytes. Additionally, the figure demonstrates that the activation of R lymphocytes helps the system achieve homeostasis after approximately 35 to 45 days, consistent with experimental data reported in the literature [28–35,38–41].

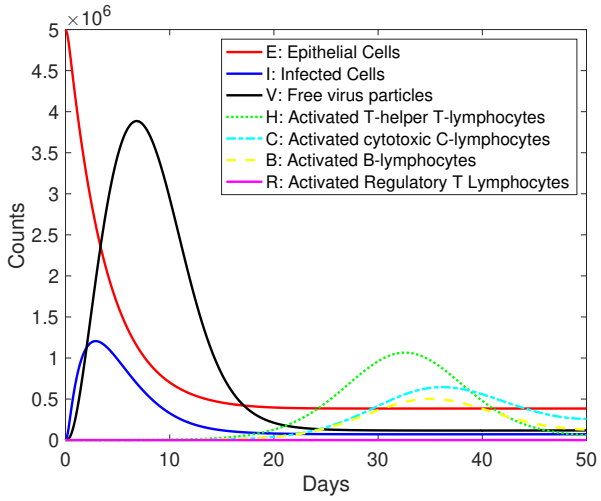

Figure 2. Viral and cellular dynamics for a viral infection given by System (3) for parameters $g_E = 10^5$, $d_E = 0.02$, $\tau_E = 0.25$, $\zeta_{VE} = 5 \times 10^3$, $d_I = 0.5$, $\tau_I = 0.8$, $\zeta_{CI} = 3 \times 10^3$, $\nu = 0.9$, $d_V = 0.05$, $\tau_V = 0.5$, $\zeta_{BV} = 2 \times 10^3$, $g_H = 50$, $d_H = 0.15$, $\rho_H = 0.85$, $\tau_H = 0.5$, $\zeta_{IH} = 100$, $\zeta_{RH} = 500$, $g_C = 50$, $d_C = 0.15$, $\rho_C = 0.65$, $\tau_C = 0.5$, $\zeta_{HC} = 500$, $\zeta_{RC} = 500$, $g_B = 50$, $d_B = 0.15$, $\rho_B = 0.7$, $\tau_B = 0.5$, $\zeta_{HB} = 500$, $\zeta_{RB} = 500$, and initial conditions $E = 5 \times 10^6$, $I = 0$, $V = 1 \times 10^3$, $H = 50$, $C = 30$, $B = 20$, $R = 5$ as in [2,17–19,32,37–40].

From the above, it is highlighted that taking into account relevant literature [28–36,41–44], suppression by R lymphocytes should occur between 25 and 35 days after the onset of infection. For this purpose, an adjustment was made to the value of the parameters, achieving a closer approximation to the expected biological process related to the immune response as shown in Figure 4.

Furthermore, it is ensured that the behavior of the R lymphocytes in Figures 2 and 4 conforms to the expected; this is observed under a scale adjustment as shown in Figures 3 and 5.

The curves represented in Figures 2 and 4 compare the dynamics with different generation rates of H lymphocytes, C lymphocytes, and B lymphocytes, according to the values of parameters g_H, g_B, and g_C and the same occurs in the elimination of these

lymphocytes in relation to the parameters d_H, d_B and d_C, proving that an increase in both the different generations and elimination of the mentioned lymphocytes leads to an early response of the immune response, as well as remaining within the established days to obtain an activation response in the established interval.

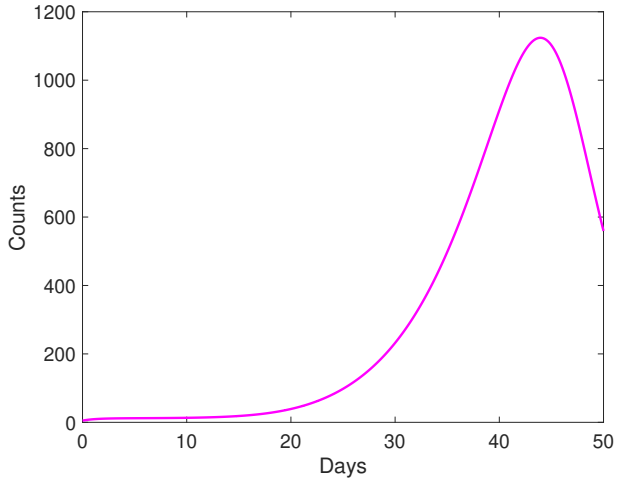

Figure 3. Dynamics of regulatory T lymphocytes activation associated to Figure 2, and using parameters $g_R = 10$, $d_R = 0.35$, $\rho_R = 0.49$, $\tau_R = 1$, $\zeta_{HR} = 4 \times 10^4$.

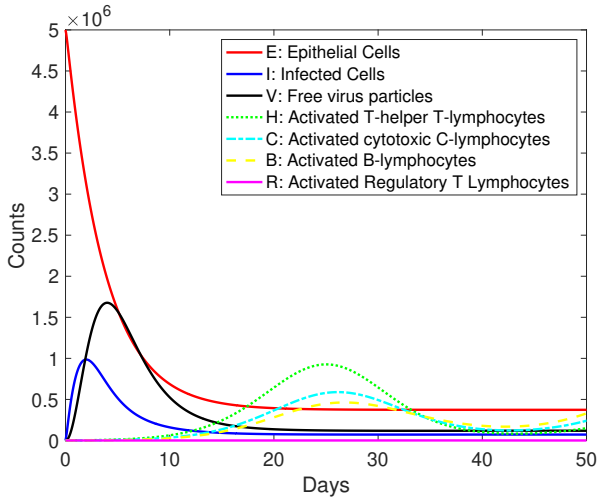

Figure 4. Viral and cellular dynamics for a viral infection described or modeling by System (3) for parameters $g_E = 10^5$, $d_E = 0.02$, $\tau_E = 0.25$, $\zeta_{VE} = 1 \times 10^3$, $d_I = 0.5$, $\tau_I = 0.8$, $\zeta_{CI} = 3 \times 10^3$, $\nu = 0.9$, $d_V = 0.05$, $\tau_V = 0.5$, $\zeta_{BV} = 2 \times 10^3$, $g_H = 1000$, $d_H = 0.175$, $\rho_H = 0.9$, $\tau_H = 0.5$, $\zeta_{IH} = 500$, $\zeta_{RH} = 500$, $g_C = 700$, $d_C = 0.185$, $\rho_C = 0.75$, $\tau_C = 0.5$, $\zeta_{HC} = 450$, $\zeta_{RC} = 450$, $g_B = 500$, $d_B = 0.175$, $\rho_B = 0.6$, $\tau_B = 0.5$, $\zeta_{HB} = 300$, $\zeta_{RB} = 300$, and initial conditions $E = 5 \times 10^6$, $I = 0$, $V = 1 \times 10^3$, $H = 50$, $C = 30$, $B = 20$, $R = 5$ as in [2,17–19,32,37–40].

Thus, it is observed that the dynamics of regulatory T lymphocytes activation (τ_R) leads to the regulation of effector functions of the lymphocytes that are acting in System (3), and an increase in regulatory T lymphocytes implies the early neutralization of these functions, which leads to the establishment of homeostasis within the organism, without leaving aside that these are still in the ranges established by the literature [33–36,43,44]

Figure 4 shows that the increased cytotoxic response in infected cells tends to decrease the amount of free viral particles, resulting in fewer infected epithelial cells. When there is increased neutralization of free viral particles, it leads to an increased antibody response of the organism, resulting in an early immune response.

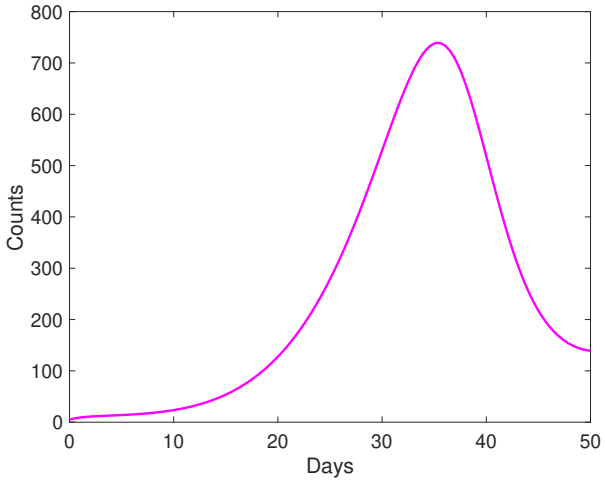

Figure 5. Dynamics of regulatory T lymphocyte activation associated to Figure 4, and using parameters $g_R = 10$, $d_R = 0.25$, $\rho_R = 0.59$, $\tau_R = 1$, $\zeta_{HR} = 5 \times 10^4$.

In other modeling work, different criteria are selected to define the severity of viral infection, such as the fraction of infected cells [2,32,37,45–49], cumulative tissue damage [22,23,50–52], damage-associated molecular patterns and pathogen-associated molecular patterns [23,29,38,50,53]. In our results, we demonstrate that individuals with an increased induced Treg effectively suppress the inflammatory response in contrast to similar cells of lower content, which is consistent with modeling studies indicating how Tregs help regulate the immune system, while activated H lymphocytes, C lymphocytes, and B lymphocytes enter a memory phase with latent capacity to respond more rapidly to the reintroduction of the same pathogen [54–56].

Basic Reproductive Number

The reproductive number for cell models, usually denoted by R_0, is defined as the number of new infected cells generated from a first infected cell when the virus is introduced into a population of susceptible cells (E) [38].

If $R_0 < 1$, it is assumed that the infection is eliminated, i.e., the virus is not able to reproduce, resulting in a viral load that tends to zero. Therefore, each virus-infected cell produces, on average, less than one new infected cell. It is then predicted that the infection will disappear from the population or that the virus will be eliminated from the individual; therefore, the infection cannot spread, and the system returns to the uninfected state.

If $R_0 > 1$, the infection progresses and the virus can invade the susceptible cell population (E).

To derive the expression of the reproductive number of System (3), the next generation matrix method [57] is used as follows:

$$R_0 = \frac{g_E(g_B+d_B\zeta_{BV})(g_C+d_C\zeta_{CI})\nu\tau_E}{d_E(d_I(g_C+d_C\zeta_{CI})+g_C\tau_I)(d_V(g_B+d_B\zeta_{BV})+g_B\tau_V)\zeta_{VE}}. \tag{4}$$

Remark. *It is specified that in an organism without the disease, that is, $V(0) = 0$ and $I(0) = 0$, this is a case where $E' = g_E - d_E E$; this implies $E(t) \to g_E/d_E$.*

We are aware that our mathematical analysis is an initial attempt to examine the activation of the immune response and may not fully account for the associated intertwined cellular communication pathways. Nevertheless, it serves as a hypothesis-building and hypothesis-provoking process that should encourage the integrated analysis of SARS-CoV-2 pathogenesis. Future experimental data examining the interrelationships between SARS-CoV-2 and the immune response will allow us to further refine our model and implement realistic parameters in the rates of systems of equations.

4. Conclusions

This paper formulated a seven-compartment mathematical model to simulate the dynamics of activation and regulation of the immune response to viral pathogens. The model includes the following state variables: epithelial cells, infected cells, free viral particles, helper T lymphocytes, cytotoxic T lymphocytes, B lymphocytes and regulatory T lymphocytes. This type of cell-mediated immune response is relevant in respiratory diseases caused by viruses such as measles and influenza, among others. The study demonstrated the positivity of the proposed model solutions, ensuring that the state variables remain positive as long as there is an initial presence of virus and infected cells in the system. In addition, an analysis of the local stability of the homogeneous system was performed, which provided essential insight into the dynamics of the state variables of the model. The results indicated that solutions tend to stabilize around an equilibrium point, which biologically implies the neutralization of viral particles and the elimination of infected cells.

Finally, the theoretical results were validated by numerical simulations using data reported in the literature on the SARS-CoV-2 virus. These simulations showed an approximation of biological behavior and provided an appropriate fit to the timing of virus transmissibility, symptom onset, antibody levels, and lymphocyte response, thus improving the understanding of the dynamics of viral infection.

Author Contributions: Conceptualization, L.C.-H., L.P. and C.M.; methodology, L.C.-H., L.P., F.C.-L., A.D.A. and C.M.; software, L.C.-H. and C.M.; validation, L.C.-H., L.P., F.C.-L., A.D.A. and C.M.; formal analysis, L.C.-H., L.P., F.C.-L. and C.M.; writing—original draft preparation, L.C.-H., L.P., F.C.-L., A.D.A. and C.M.; writing—review and editing, L.C.-H., L.P., F.C.-L., A.D.A. and C.M.; supervision, L.C.-H. All authors have read and agreed to the published version of the manuscript.

Funding: This work was funded by a research project of the Agencia Nacional de Investigación y Desarrollo (ANID) of Chile, FONDECYT Regular #1231256.

Data Availability Statement: Data are contained within the article.

Acknowledgments: L. Cuesta-Herrera thanks the "UCM Doctoral Scholarship" from the Vice-Rectory for Research and Postgraduate Studies, as well as to the PhD Program in Applied Mathematical Modeling at Universidad Católica del Maule, Talca, Chile; the Mathematical Modelling Research Group, and the PhD Program in Mathematical Engineering at Universidad EAFIT, Medellín, Colombia.

Conflicts of Interest: The authors declare that they have no known competing financial interests or personal relationships that could have appeared to influence the work reported in this paper.

Appendix A. Positivity of a Homogeneous System

In this Appendix A, the definitions and properties necessary to preserve the positivity of system homogeneous Ordinary Differential Equations (ODEs) will be presented in System (A1).

Let the ODEs system be non-linear and self-contained

$$\begin{cases} Y' = A(Y) \cdot Y, \\ Y(0) = Y_0 \in \mathbb{R}^n, \end{cases} \tag{A1}$$

where the matrix $A : \mathbb{R}^n \to \mathbb{R}^{n \times n}$ is a weak Laplacian graph, which is defined as follows.

Definition A1. *$A_{n\times n}$ is a **weak Laplacian graph** if it satisfies the following property:*

Property A1. *(pattern of signs) $A_{k,l} \geq 0$, for $k, l = 1, 2, ..., n, k \neq l$ and $A_{k,k} \leq 0$ for $k = 1, 2, ..., n$.*

The definition of the laplacian graph involves an additional property dealing with mass conservation, which is not relevant to our work, see [58].

The definition of cone is given below and can be found at [59,60].

Definition A2. *Let $A \subset \mathbb{R}^m$. If Λ is a nonempty subset of $\mathbb{R}$, then $\Lambda A = \bigcup_{\lambda\in\Lambda} \lambda A := \bigcup_{\lambda\in\Lambda} \{\lambda a | a \in A\}$. A set $A \subset \mathbb{R}^m$ is a cone (sometimes called a non-negative cone) if $A = \mathbb{R}_+ A$, where $\mathbb{R}_+ := \{\lambda \in \mathbb{R} | \lambda > 0\}$. In other words, a cone is a subset of a vector space that is closed under positive scalar multiplication.*

In order to establish the main results, we define the relationship between the matrices as follows.

Definition A3. *Given two compatible matrices P and Q, we say that:*

$P \succ Q$ if $P_{i,j} > Q_{i,j}$ for all i, j and
$P \succeq Q$ if $P_{i,j} \geq Q_{i,j}$ for all i, j.

With the definitions given above, the following result is obtained.

Proposition A1. *System solutions (A1) with $Y_0 \succeq \mathbf{0}$ preserve positivity, i.e., $Y(t) \succeq \mathbf{0}$ for all $t \geq 0$.*

Proof. First we will test the positivity of System (A1). For any $t^* \geq 0$ such that exists $k^* \in \{1, 2, \ldots, n\}$ with $Y_{k^*}(t^*) = 0$ and $Y(t^*) \succeq \mathbf{0}$, if t^* there is, $Y(t)$ is contained in a non-negative cone. By (A1), it follows that

$$Y'_{k^*}(t^*) = \sum_{l=1}^{n} A_{k^*,l}(Y(t^*)) \cdot Y_l(t^*) \geq 0, \tag{A2}$$

since A is a Laplacian graph, hence the off-diagonal elements are non-negative. Therefore, Y_{k^*} cannot change sign in t^*, hence Y_{k^*} must belong to the non-negative cone. □

In the case of a non-homogeneous ODE System (A3)

$$\begin{cases} Y' = A(Y) \cdot Y + b, \\ Y(0) = Y_0 \in \mathbb{R}^n, \end{cases} \tag{A3}$$

where, $b \in \mathbb{R}^n$ is the independent term, positivity is still preserved if $b \succeq \mathbf{0}$ and similarly to the homogeneous case.

Although the previous approach is applicable for $b \succeq \mathbf{0}$, additional hypotheses on cell biological behavior (number of Epithelial cells, viral particles and lymphocytes) arise to keep the system in self-tolerance and homeostasis. That is, from a mathematical point of view following conditions are sufficient:

$$\frac{I\tau_H}{\zeta_{IH}+I} < d_H + \frac{\rho_H R}{\zeta_{RH}+R}, \quad \frac{\tau_C H}{\zeta_{HC}+H} < d_C + \frac{\rho_C R}{\zeta_{RC}+R}, \quad \frac{\tau_B H}{\zeta_{HB}+H} < d_B + \frac{\rho_B R}{\zeta_{RB}+R}, \quad \frac{\tau_R H}{\zeta_{HR}+H} < d_R + \rho_R.$$

Which imply that the solutions of System (A4) with non-negative initial condition preserve positivity.

In Appendix B, we present an alternative proof for the non-homogeneous case, specifically for System (3).

Appendix B. Positivity of a Non-Homogeneous System

In this appendix, we will prove the positivity of System (3). Furthermore, taking into account the formulation proposed in Appendix A, we will describe System (3) as a system of non-homogeneous autonomous Ordinary Differential Equations (ODEs), given by

$$\begin{cases} Y' = A(Y) \cdot Y + b, \\ Y(0) = Y_0 = (E_0, I_0, V_0, H_0, C_0, B_0, R_0)^\top, \end{cases} \tag{A4}$$

where the sign $\top$ is the transpose of the initial vector and

$$A(Y) = \begin{pmatrix} L_1 & 0 & 0 & 0 & 0 & 0 & 0 \\ \frac{\tau_E V}{\zeta_{VE}+V} & L_2 & 0 & 0 & 0 & 0 & 0 \\ 0 & \nu & L_3 & 0 & 0 & 0 & 0 \\ 0 & 0 & 0 & L_4 & 0 & 0 & 0 \\ 0 & 0 & 0 & 0 & L_5 & 0 & 0 \\ 0 & 0 & 0 & 0 & 0 & L_6 & 0 \\ 0 & 0 & 0 & 0 & 0 & 0 & L_7 \end{pmatrix}, \tag{A5}$$

with

$$\begin{aligned} L_1 &= -d_E - \frac{\tau_E V}{\zeta_{VE}+V}, \\ L_2 &= -\frac{C\tau_I}{C+\zeta_{CI}} - d_I, \\ L_3 &= -\frac{\tau_V B}{B+\zeta_{BV}} - d_V, \\ L_4 &= -d_H - \frac{\rho_H R}{\zeta_{RH}+R} + \frac{I\tau_H}{\zeta_{IH}+I}, \\ L_5 &= -d_C - \frac{\rho_C R}{\zeta_{RC}+R} + \frac{\tau_C H}{\zeta_{HC}+H}, \\ L_6 &= -d_B - \frac{\rho_B R}{\zeta_{RB}+R} + \frac{\tau_B H}{\zeta_{HB}+H}, \\ L_7 &= -d_R - \rho_R + \frac{\tau_R H}{\zeta_{HR}+H}, \end{aligned}$$

and

$$b = (g_E, 0, 0, g_H, g_C, g_B, g_R)^\top \geq (0,0,0,0,0,0,0)^\top, \tag{A6}$$

where b represents the generation of epithelial cells and lymphocytes in a state of cell turnover, assuming a basal state with no infected cells ($I_0 = 0$).

Next, the positivity of System (3) is tested.

Proposition A2. *The solutions of System (A4) with* $Y_0 \succeq (0,0,0,0,0,0,0)^\top$ *are positive, i.e.,* $Y(t) \succeq \mathbf{0}$ *for all* $t \geq 0$.

Proof. According to the theorem of the existence and uniqueness of the solution of the Cauchy problem (A4), on some interval $[0, t_1)$, a solution consisting of components $E(t)$, $I(t)$, $V(t)$, $H(t)$, $C(t)$, $B(t)$ and $R(t)$ is defined. We will assume that the corresponding initial conditions $E_0, I_0, V_0, H_0, C_0, B_0, R_0$ are non-negative. Also, we will assume that $I_0, V_0 > 0$. Let us substitute the obtained solution into the system of differential equations. It is easy to see that the equations for the components $E(t), H(t), C(t), B(t), R(t)$ together with the corresponding initial conditions E_0, H_0, C_0, B_0, R_0 can be written as a set of Cauchy problems of the form:

$$x'(t) = \kappa - a(t)x(t), \quad x(0) = x_0 \geq 0,$$

where $a(t)$ is a given function defined on the interval $[0, t_1)$ and κ is a positive heterogeneity. For example, for the first differential equation, we have:

$$a(t) = d_E + \tau_E \frac{V(t)}{V(t)+\zeta_{VE}}, \quad \kappa = g_E > 0.$$

Such a Cauchy problem is easily integrated over an interval $[0, t_1)$, for example, by the variation of the constant method. From the corresponding formula for solving this Cauchy problem, it follows that $x(t) > 0$ for all $t \in (0, t_1)$. Thus, all components $E(t), H(t), C(t), B(t), R(t)$ are positive for all $t \in (0, t_1)$.

It remains to show that the components $I(t)$ and $V(t)$ are also positive for these values of t. The corresponding Cauchy problem for these functions takes the form:

$$I'(t) = b(t)\frac{V(t)}{V(t) + \zeta_{VE}} - a_1(t)I(t), \quad I(0) = I_0 > 0,$$

$$V'(t) = \nu I(t) - a_2(t)V(t), \quad V(0) = V_0 > 0.$$

Here, $b(t) = \tau_E E(t)$, $a_1(t) = d_I + \tau_I \frac{C(t)}{C(t)+\zeta_{CI}}$ and $a_2(t) = d_V + \tau_V \frac{B(t)}{B(t)+\zeta_{BV}}$. Note that the functions $I(t)$ and $V(t)$ cannot simultaneously vanish for some $t_0 \in (0, t_1)$. Otherwise, according to the existence and uniqueness theorem, we have the equality $I(t) = V(t) = 0$ that holds for all $t \in [0, t_1)$, which is contradictory. Next, let us consider two possible cases.

- Case 1: $I(t_0) = 0$, $I(t) > 0$ for all $t \in [0, t_0)$, $I'(t_0) \leq 0$. In addition, $V(t) > 0$ for all $t \in [0, t_0)$. From the first equation of the Cauchy problem above, we have $I'(t_0) = b(t_0)\frac{V(t_0)}{V(t_0)+\zeta_{VE}} > 0$. We have a contradiction, and such a case is impossible.
- Case 2: $V(t_0) = 0$, $V(t) > 0$ for all $t \in [0, t_0)$, $V'(t_0) \leq 0$. In addition, $I(t) > 0$ for all $t \in [0, t_0)$. From the second equation of the Cauchy problem above, we have $V'(t_0) = \nu I(t_0) > 0$. We again have a contradiction, and such a case is also impossible.

This means that the functions $I(t)$ and $V(t)$ do not vanish on the interval $[0, t_1)$ and they are also positive. Therefore, $Y(t) = (E(t), I(t), V(t), H(t), C(t), B(t), R(t))^\top \succeq \mathbf{0}$ for all $t \geq 0$. □

The previous result shows that all solutions of the non-homogeneous System (3) remain positive over time ($t \geq 0$). This means that the quantities modeled, such as the number of epithelial cells, viral particles, and lymphocytes, never become negative, provided there is an initial presence of virus and infected cells in the model.

Appendix C. Stability

Note that studying the stability of a homogeneous system will provide a fundamental understanding of the dynamics of the state variables of System (3). In this appendix, we will study the stability of the homogeneous System (A7), given by:

$$\begin{cases} E' = -\left(d_E + \tau_E \frac{V}{V+\zeta_{VE}}\right)E, \\ I' = \tau_E \frac{VE}{V+\zeta_{VE}} - \left(d_I + \tau_I \frac{C}{C+\zeta_{CI}}\right)I, \\ V' = \nu I - \left(d_V + \tau_V \frac{B}{B+\zeta_{BV}}\right)V, \\ H' = -\left(d_H - \tau_H \frac{I}{I+\zeta_{IH}} + \rho_H \frac{R}{R+\zeta_{RH}}\right)H, \\ C' = -\left(d_C - \tau_C \frac{H}{H+\zeta_{HC}} + \rho_C \frac{R}{R+\zeta_{RC}}\right)C, \\ B' = -\left(d_B - \tau_B \frac{H}{H+\zeta_{HB}} + \rho_B \frac{R}{R+\zeta_{RB}}\right)B, \\ R' = -\left(d_R - \tau_R \frac{H}{H+\zeta_{HR}} + \rho_R\right)R. \end{cases} \tag{A7}$$

First, by equating all the equations of System (A7) to zero, we have that the origin $\mathbf{0} = (0, 0, 0, 0, 0, 0, 0)^\top$ is the only point of equilibrium.

Now, we present a stability result associated to the homogeneous System (A7).

Proposition A3. *The origin of the homogeneous System (A7) is locally asymptotically stable.*

Proof. First, we calculate the Jacobian of the homogeneous System (A7), J, given by

$$J = \begin{pmatrix} L_1 & 0 & -\frac{E\zeta_V E\tau_E}{(\zeta_{VE}+V)^2} & 0 & 0 & 0 & 0 \\ \frac{\tau_E V}{\zeta_{VE}+V} & L_2 & \frac{E\zeta_{VE}\tau_E}{(\zeta_{VE}+V)^2} & 0 & -\frac{\zeta_{CI} I\tau_I}{(C+\zeta_{CI})^2} & 0 & 0 \\ 0 & \nu & L_3 & 0 & 0 & -\frac{\zeta_{BV}\tau_V V}{(B+\zeta_{BV})^2} & 0 \\ 0 & \frac{\zeta_{IH} H\tau_H}{(\zeta_{IH}+I)^2} & 0 & L_4 & 0 & 0 & -\frac{\zeta_{RH} H\rho_H}{(\zeta_{RH}+R)^2} \\ 0 & 0 & 0 & \frac{C\zeta_{HC}\tau_C}{(\zeta_{HC}+H)^2} & L_5 & 0 & -\frac{C\zeta_{RC}\rho C}{(\zeta_{RC}+R)^2} \\ 0 & 0 & 0 & \frac{B\zeta_{HB}\tau_B}{(\zeta_{HB}+H)^2} & 0 & L_6 & -\frac{B\zeta_{RB}\rho_B}{(\zeta_{RB}+R)^2} \\ 0 & 0 & 0 & \frac{\zeta_{HR} R\tau_R}{(\zeta_{HR}+H)^2} & 0 & 0 & L_7 \end{pmatrix}. \tag{A8}$$

Now, evaluating the Jacobian at the origin, we have that

$$J(\mathbf{0}) = \begin{pmatrix} -d_E & 0 & 0 & 0 & 0 & 0 & 0 \\ 0 & -d_I & 0 & 0 & 0 & 0 & 0 \\ 0 & \nu & -d_V & 0 & 0 & 0 & 0 \\ 0 & 0 & 0 & -d_H & 0 & 0 & 0 \\ 0 & 0 & 0 & 0 & -d_C & 0 & 0 \\ 0 & 0 & 0 & 0 & 0 & -d_B & 0 \\ 0 & 0 & 0 & 0 & 0 & 0 & -d_R - \rho_R \end{pmatrix}, \tag{A9}$$

whose eigenvalues are given by

$$\lambda_1 = -d_B, \quad \lambda_2 = -d_C, \quad \lambda_3 = -d_E,$$

$$\lambda_4 = -d_H, \quad \lambda_5 = -d_I, \quad \lambda_6 = -d_V, \quad \text{and} \quad \lambda_7 = -(d_R + \rho_R).$$

Clearly, all eigenvalues are negative. Therefore, the origin is an equilibrium point that is locally asymptotically stable. □

Since the solutions of the homogeneous System (A7) will tend to stabilize around the equilibrium point, biologically, this means that the viral particles are neutralized, and infected cells are eliminated.

References

1. Pincheira-Brown, P.; Bentancor, A. Forecasting COVID-19 infections with the semi-unrestricted generalized growth model. *Epidemics.* **2021**, *37*, 100486. [CrossRef] [PubMed]
2. Wang, S.; Pan, Y.; Wang, Q.; Miao, H.; Brown, A.N.; Libin Rong. Modeling the viral dynamics of SARS-CoV-2 infection. *Math. Biosci.* **2020**, *328*, 108438. ISSN 0025-5564. [CrossRef] [PubMed]
3. Du, S.Q.; Yuan, W. Mathematical modeling of interaction between innate and adaptive immune responses in COVID-19 and implications for viral pathogenesis. *J. Med. Virol.* **2020**, *92*, 1615–1628. [CrossRef] [PubMed]
4. Vetter, P.; Eberhardt, C.S.; Meyer, B.; Martinez Murillo, P.A.; Torriani, G.; Pigny, F.; Lemeille, S.; Cordey, S.; Laubscher, F.; Vu, D.-L.; et al. Daily viral kinetics and innate and adaptive immune response assessment in COVID-19: A case series. *mSphere* **2020**, *5*, e00827-20. [CrossRef] [PubMed]
5. Kamae, I. A theory of diagnostic testing to stop the virus spreading: Evidence-based reasoning to resolve the COVID-19 crisis by testing. *Keio J. Med.* **2022**, *71*, 13–20. [CrossRef]
6. Pal, M.; Berhanu, G.; Desalegn, C.; Kandi, V. Severe acute respiratory syndrome coronavirus-2 (SARS-CoV-2): An update. *Cureus* **2020**, *12*, e7423. [CrossRef]
7. Abduljalil, J.M.; Abduljalil, B.M. Epidemiology, genome, and clinical features of the pandemic SARS-CoV-2: A recent view. *New Microbes New Infect.* **2020**, *35*, 100672. [CrossRef]
8. Larsen, J.R.; Martin, M.R.; Martin, J.D.; Hicks, J.B.; Kuhn, P. Modeling the onset of symptoms of COVID-19: Effects of SARS-CoV-2 variant. *PLoS Comput. Biol.* **2021**, *17*, e1009629. [CrossRef]
9. Chen, J.; Wang, R.; Wang, M.; Wei, G.-W. Mutations strengthened SARS-CoV-2 infectivity. *J. Mol. Biol.* **2020**, *432*, 5212–5226. [CrossRef]
10. Layton, A.T.; Sadria, M. Understanding the dynamics of SARS-CoV-2 variants of concern in ontario, canada: A modeling study. *Sci. Rep.* **2022**, *12*, 1–16.
11. Chen, J.; Wang, R.; Gilby, N.B.; Wei, G.-W. Omicron variant (b. 1.1. 529): Infectivity, vaccine breakthrough, and antibody resistance. *J. Chem. Inf. Model.* **2022**, *62*, 412–422. [CrossRef] [PubMed]

12. Kannan, S.; Ali, P.S.S.; Sheeza, A. Evolving biothreat of variant SARS-CoV-2-molecular properties, virulence and epidemiology. *Eur. Rev. Med. Pharmacol. Sci.* **2021**, *25*, 4405–4412. [PubMed]
13. De, R.; Dutta, S. Role of the microbiome in the pathogenesis of COVID-19. *Front. Cell. Infect. Microbiol.* **2022**, *12*, 736397. [CrossRef] [PubMed]
14. Baric, R.S. Emergence of a highly fit SARS-CoV-2 variant. *N. Engl. J. Med.* **2020**, *383*, 2684–2686. [CrossRef] [PubMed]
15. Maher, M.C.; Bartha, I.; Weaver, S.; Iulio, J.D.; Ferri, E.; Leah S.; Lempp, F.A.; Hie, B.L.; Bryson, B.; Berger, B.; et al. Predicting the mutational drivers of future SARS-CoV-2 variants of concern. *Sci. Transl. Med.* **2022**, *14*, eabk3445. [CrossRef]
16. Cuesta-Herrera, L.; Córdova-Lepe, F.; Pastenes, L.; Arencibia, A.D.; Baldera-Moreno, Y.; Torres-Mantilla, H.A. A mathematical model and simulation scenarios for t and b cells immune response to severe acute respiratory syndrome-coronavirus-2. In *Journal of Physics: Conference Series*; IOP Publishing: Bristol, UK, 2023; Volume 2516, p. 012007.
17. Kuklina, E.M. T lymphocytes as targets for SARS-CoV-2. *Biochemistry* **2022**, *87*, 566–576. [CrossRef]
18. Gualana, F.L.; Maiorca, F.; Marrapodi, R.; Villani, F.; Miglionico, M.; Santini, S.A.; Pulcinelli, F.; Gragnani, L.; Piconese, S.; Fiorilli, M.; et al. Opposite effects of mrna-based and adenovirus-vectored SARS-CoV-2 vaccines on regulatory t cells: A pilot study. *Biomedicines* **2023**, *11*, 511. [CrossRef]
19. Samaan, E.; Elmaria, M.O.; Khedr, D.; Gaber, T.; Elsayed, A.G.; N Shenouda, R.; Gamal, H.; Shahin, D.; Abousamra, N.K.; Shemies, R. Characterization of regulatory t cells in SARS-CoV-2 infected hemodialysis patients: Relation to clinical and radiological severity. *BMC Nephrol.* **2022**, *23*, 391. [CrossRef]
20. Walter, L.O.; Cardoso, C.C.; Santos-Pirath, I.M.; Costa, H.Z.; Gartner, R.; Werle, I.; Bramorski Mohr, E.T.; da Rosa, J.S.; Lubschinski, T.L.; Felisberto, M.; et al. T cell maturation is significantly affected by SARS-CoV-2 infection. *Immunology* **2023**, *169*, 358–368. [CrossRef]
21. Chaple, A.R.; Vispute, M.M.; Mahajan, S.; Mushtaq, S.; Muthuchelvan, D.; Ramakrishnan, M.A.; Kumar Sharma, G. Relational interaction between t-lymphocytes and SARS-CoV-2: A review. *Acta Virol.* **2021**, *65*, 107–114. [CrossRef]
22. Gonçalves, A.; Bertrand, J.; Ke, R.; Comets, E.; Lamballerie, X.; Malvy, D.; Pizzorno, A.; Terrier, O.; Calatrava, M.R.; Mentré, F.; et al. Timing of antiviral treatment initiation is critical to reduce SARS-CoV-2 viral load. *CPT Pharmacometrics Syst. Pharmacol.* **2020**, *9*, 509–514. [CrossRef] [PubMed]
23. Pawelek, K.A.; Dor, D., Jr.; Salmeron, C.; Handel, A. Within-host models of high and low pathogenic influenza virus infections: The role of macrophages. *PLoS ONE* **2016**, *11*, e0150568. [CrossRef]
24. Goyal, A.; Cardozo-Ojeda, E.F.; Schiffer, J.T. Potency and timing of antiviral therapy as determinants of duration of SARS-CoV-2 shedding and intensity of inflammatory response. *Sci. Adv.* **2020**, *6*, eabc7112. [CrossRef]
25. McCallum, H.; Barlow, N.; Hone, J. How should pathogen transmission be modelled? *Trends Ecol. Evol.* **2001**, *16*, 295–300. [CrossRef]
26. Fischer, D.S.; Ansari, M.; Wagner, K.I.; Jarosch, S.; Huang, Y.; Mayr, C.H.; Strunz, M.; Lang, N.J.; D'Ippolito, E.; Hammel, M.; et al. Single-cell rna sequencing reveals ex vivo signatures of SARS-CoV-2-reactive t cells through 'reverse phenotyping'. *Nat. Commun.* **2021**, *12*, 1–14. [CrossRef] [PubMed]
27. He, Z.; Zhao, C.; Dong, Q.; Zhuang, H.; Song, S.; Peng, G.; Dwyer, D.E. Effects of severe acute respiratory syndrome (sars) coronavirus infection on peripheral blood lymphocytes and their subsets. *Int. J. Infect. Dis.* **2005**, *9*, 323–330. [CrossRef] [PubMed]
28. Laferl, H.; Kelani, H.; Seitz, T.; Holzer, B.; Zimpernik, I.; Steinrigl, A.; Schmoll, F.; Wenisch, C.; Allerberger, F. An approach to lifting self-isolation for health care workers with prolonged shedding of SARS-CoV-2 RNA. *Infection* **2021**, *49*, 95–101. [CrossRef]
29. Singanayagam, A.; Patel, M.; Charlett, A.; Bernal, J.L.; Saliba, V.; Ellis, J.; Ladhani, S.; Zambon, M.; Gopal, R. Duration of infectiousness and correlation with rt-pcr cycle threshold values in cases of COVID-19, england, january to may 2020. *Eurosurveillance* **2020**, *25*, 2001483. [CrossRef]
30. Sohn, Y.; Jeong, S.J.; Chung, W.S.; Hyun, J.H.; Baek, Y.J.; Cho, Y.; Kim, J.H.; Ahn, J.Y.; Choi, J.Y.; Yeom, J.-S. Assessing viral shedding and infectivity of asymptomatic or mildly symptomatic patients with COVID-19 in a later phase. *J. Clin. Med.* **2020**, *9*, 2924. [CrossRef]
31. Rhee, C.; Kanjilal, S.; Baker, M.; Klompas, M. Duration of severe acute respiratory syndrome coronavirus 2 (SARS-CoV-2) infectivity: When is it safe to discontinue isolation? *Clin. Infect. Dis.* **2021**, *72*, 1467–1474. [CrossRef]
32. Challenger, J.D.; Foo, C.Y.; Wu, Y.; Yan, A.W.; Marjaneh, M.M.; Liew, F.; Thwaites, R.S.; Okell, L.C.; Cunnington, A.J. Modelling upper respiratory viral load dynamics of SARS-CoV-2. *BMC Med.* **2022**, *20*, 1–20. [CrossRef]
33. Ghostine, R.; Gharamti, M.; Hassrouny, S.; Hoteit, I. Mathematical modeling of immune responses against SARS-CoV-2 using an ensemble kalman filter. *Mathematics*. **2021**, *9*, 2427. [CrossRef]
34. Hattaf, K.; Yousfi, N. Dynamics of SARS-CoV-2 infection model with two modes of transmission and immune response. *Math. Biosci. Eng.* **2020**, *17*, 5326–5340. [CrossRef] [PubMed]
35. Chatterjee, A.N.; Basir, F.A.; Almuqrin, M.A.; Mondal, J.; Khan, I. SARS-CoV-2 infection with lytic and non-lytic immune responses: A fractional order optimal control theoretical study. *Results Phys.* **2021**, *26*, 104260. [CrossRef] [PubMed]
36. Sante, G.D.; Buonsenso, D.; Rose, C.D.; Tredicine, M.; Palucci, I.; Maio, F.D.; Camponeschi, C.; Bonadia, N.; Biasucci, D.; Pata, D.; et al. Immunopathology of SARS-CoV-2 infection: A focus on t regulatory and b cell responses in children compared with adults. *Children* **2022**, *9*, 681. [CrossRef]
37. Hernandez-Vargas, E.A.; Velasco-Hernandez, J.X. In-host mathematical modelling of COVID-19 in humans. *Annu. Rev. Control.* **2020**, *50*, 448–456. ISSN 1367-5788. [CrossRef]

38. Abuin, P.; Anderson, A.; Ferramosca, A.; Hernandez-Vargas, E.A.; Gonzalez, A.H. Characterization of SARS-CoV-2 dynamics in the host. *Annu. Rev. Control.* **2020**, *50*, 457–468. ISSN 1367-5788. [CrossRef]
39. Wölfel, R.; Corman, V.M.; Guggemos, W.; Seilmaier, M.; Zange, S.; Müller, M.A.; Niemeyer, D.; Jones, T.C.; Vollmar, P.; Rothe, C.; et al. Virological assessment of hospitalized patients with COVID-2019. *Nature.* **2020**, *581*, 465–469. [CrossRef]
40. Tyrrell, D.A.J.; Myint, S.H. Coronaviruses. University of Texas Medical Branch at Galveston. 1996. Available online: http://www.ncbi.nlm.nih.gov/pubmed/21413266 (accessed on 1 June 2021).
41. Cuesta-Herrera, L.; Pastenes, L.; Córdova-Lepe, F.; Arencibia, A.D.; Torres-Mantilla, H.A. Cell lysis analysis for respiratory viruses through simulation modeling. In *Journal of Physics: Conference Series*; IOP Publishing: Bristol, UK, 2022; Volume 2159, p. 012002.
42. Cuesta-Herrera, L.; Pastenes, L.; Córdova-Lepe, F.; Arencibia, A.D.; Torres-Mantilla, H.; Gutiérrez-Jara, J.P. Analysis of seir-type models used at the beginning of COVID-19 pandemic reported in high-impact journals. *Medwave* **2022**, *22*, 2552. [CrossRef]
43. Uçaryilmaz, H.; Ergün, D.; Vatansev, H.; Köksal, H.; Ural, O.; Arslan, U.; Artac, H. The role of cd8+ regulatory t cells and b cell subsets in patients with COVID-19. *Turk. J. Med. Sci.* **2022**, *52*, 888–898. [CrossRef]
44. Fenizia, C.; Cetin, I.; Mileto, D.; Vanetti, C.; Saulle, I.; Giminiani, M.D.; Saresella, M.; Parisi, F.; Trabattoni, D.; Clerici, M.; et al. Pregnant women develop a specific immunological long-lived memory against SARS-CoV-2. *Front. Immunol.* **2022**, *13*, 827889. [CrossRef]
45. Perelson, A.S. Modelling viral and immune system dynamics. *Nat. Rev. Immunol.* **2002**, *2*, 28–36. [CrossRef] [PubMed]
46. Ciupe, S.M.; Heffernan, J.M. In-host modeling. *Infect. Dis. Model.* **2017**, *2*, 188–202. ISSN 2468-0427. [CrossRef] [PubMed]
47. Blanco-Rodríguez, R.; Du, X.; Hernández-Vargas, E. Computational simulations to dissect the cell immune response dynamics for severe and critical cases of SARS-CoV-2 infection. *Comput. Methods Programs Biomed.* **2021**, *211*, 106412. [CrossRef] [PubMed]
48. Wang, S.; Hao, M.; Pan, Z.; Lei, J.; Zou, X. Data-driven multi-scale mathematical modeling of SARS-CoV-2 infection reveals heterogeneity among COVID-19 patients. *PLoS Comput. Biol.* **2021**, *17*, e1009587. [CrossRef] [PubMed]
49. Jenner, A.L.; Aogo, R.A.; Alfonso, S.; Crowe, V.; Deng, X.; Smith, A.P.; Morel, P.A.; Davis, C.L.; Smith, A.M.; Craig, M. COVID-19 virtual patient cohort suggests immune mechanisms driving disease outcomes. *PLoS Pathog.* **2021**, *17*, e1009753. [CrossRef]
50. Walsh, K.A.; Jordan, K.; Clyne, B.; Rohde, D.; Drummond, L.; Byrne, P.; Ahern, S.; Carty, P.G.; O'Brien, K.K.; O'Murchu, E.; et al. SARS-CoV-2 detection, viral load and infectivity over the course of an infection. *J. Infect.* **2020**, *81*, 357–371. ISSN 0163-4453. [CrossRef]
51. Baral, S.; Antia, R.; Dixit, N.M. A dynamical motif comprising the interactions between antigens and cd8 t cells may underlie the outcomes of viral infections. *Proc. Natl. Acad. Sci. USA* **2019**, *116*, 17393–17398. [CrossRef]
52. Chatterjee, B.; Sandhu, H.S.; Dixit, N.M. Modeling recapitulates the heterogeneous outcomes of SARS-CoV-2 infection and quantifies the differences in the innate immune and cd8 t-cell responses between patients experiencing mild and severe symptoms. *PLoS Pathog.* **2022**, *18*, e1010630. [CrossRef]
53. Sanche, S.; Cassidy, T.; Chu, P.; Perelson, A.S.; Ribeiro, R.M.; Ke, R. A simple model of COVID-19 explains disease severity and the effect of treatments. *Sci. Rep.* **2022**, *12*, 14210. [CrossRef]
54. Owen, J.A.; Punt, J.; Stranford, S.A.; Jones, P.P. *Kuby Immunology*; WH Freeman: New York, NY, USA, 2013.
55. Liu, Y.; Yan, L.-M.; Wan, L.; Xiang, T.-X.; Le, A.; Liu, J.-M.; Peiris, M.; Poon, L.L.M.; Zhang, W. Viral dynamics in mild and severe cases of COVID-19. *Lancet Infect. Dis.* **2020**, *20*, 656–657. [CrossRef]
56. Zhou, Z.; Li, D.; Zhao, Z.; Shi, S.; Wu, J.; Li, J.; Zhang, J.; Gui, K.; Zhang, Y.; Ouyang, Q.; et al. Dynamical modelling of viral infection and cooperative immune protection in COVID-19 patients. *PLoS Comput. Biol.* **2023**, *19*, e1011383. [CrossRef] [PubMed]
57. den Driessche, P.; Watmough, J. Reproduction numbers and sub-threshold endemic equilibria for compartmental models of disease transmission. *Math. Biosci.* **2002**, *180*, 29–48. ISSN 0025-5564. [CrossRef] [PubMed]
58. Blanes, S.; Iserles, A.; Macnamara, S. Positivity-preserving methods for ordinary differential equations. *ESAIM Math. Model. Numer. Anal.* **2022**, *56*, 1843–1870. [CrossRef]
59. Bernstein, D.S. *Matrix Mathematics*; Princeton University Press: Princeton, NJ, USA, 2009.
60. Bauschke, H.H.; Combettes, P.L. *Convex Analysis and Monotone Operator Theory in Hilbert Spaces, Corrected Printing*; Springer: New York, NY, USA, 2019.